Article

Using Saildrones to Validate Satellite-Derived Sea Surface Salinity and Sea Surface Temperature along the California/Baja Coast

Jorge Vazquez-Cuervo [1], Jose Gomez-Valdes [2], Marouan Bouali [3], Luis E. Miranda [2], Tom Van der Stocken [1] and Wenquing Tang [1], Chelle Gentemann [4]

[1] Jet Propulsion Laboratory, California Institute of Technology, Pasadena, CA 91109, USA; tom.van.der.stocken@jpl.nasa.gov (T.V.d.S.); wenqing.tang@jpl.nasa.gov (W.T.)

[2] Physical Oceanography Department, Center for Scientific Research and Higher Education at Ensenada, 22860 Ensenada, Baja California, Mexico; jgomez@cicese.mx(J.G.-V.); lmiranda@cicese.edu.mx(L.E.M.)

[3] University of Sao Paulo, Sao Paulo, Brazil; marouanbouali@gmail.com

[4] Earth and Space Research,2101 Fourth Avenue, Suite 1310, Seattle, Washington, 98121 cgentemann@esr.org

*Correspondence: jorge.vazquez@jpl.nasa.gov; Tel.: +1-818-354-6980

Abstract: Traditional ways of validating satellite-derived sea surface temperature (SST) and sea surface salinity (SSS) products, using comparisons with buoy measurements, do not allow for evaluating the impact of mesoscale to submesoscale variability. Here we present the validation of remotely-sensed SST and SSS data against the unmanned surface vehicle (USV) – Saildrone – measurements from the Spring 2018 Baja deployment. More specifically, biases and root mean square differences (RMSD) were calculated between USV-derived SST and SSS values, and six satellite-derived SST (MUR, OSTIA, CMC, K10, REMSS, and DMI) and three SSS (JPLSMAP, RSS40, RSS70) products. Biases between the USV SST and OSTIA/CMC/DMI were approximately zero while MUR showed a bias of 0.2°C. OSTIA showed the smallest RMSD of 0.36°C while DMI had the largest RMSD of 0.5°C. An RMSD of 0.4°C between Saildrone SST and the satellite-derived products could be explained by the daily variability in USV SST which currently cannot be resolved by remote sensing measurements. For SSS, values from the JPLSMAP product showed saltier biases of 0.2 PSU, while RSS40 and RSS70 showed fresh biases of 0.3 PSU. An RMSD of 0.4 PSU could not be explained solely by the daily variability of the USV-derived SSS. Coherences were significant at the longer wavelengths, with a local maximum at 100 km that is most likely associated with the mesoscale turbulence in the California Current System.

Keywords: MODIS; oceanography; remote sensing; Saildrone; sea surface salinity; sea surface temperature; SMAP; validation

1. Introduction

As a motivating factor in the study, the application of remote sensing techniques for understanding coastal and open-ocean surface water properties is an area of active research, helping to better understand oceanic structures like eddies and fronts. These features are associated with upwelling and downwelling and have been recognized to play an important role in shaping physical and biogeochemical processes in the ocean [1], and influence the spatiotemporal variability in primary productivity levels [2,3]. Typically, these mesoscale and submesoscale features reveal a clear signature in sea surface temperature (SST) [4] and sea surface salinity (SSS) [5]. Hence, continued efforts are needed to characterize and observe these structures and improve the validation quality of remotely sensed SST and SSS observations.

Traditionally, the validation of SST and SSS data has been achieved by direct comparisons with oceanic buoy measurements [6,7,8]. However, this approach does not allow for determining how well remote sensing data is resolving the spatial variability at the mesoscale to submesoscale. A reprocessing of the Advanced Very High Resolution Radiometer (AVHRR) dataset, from 9 km to 4

km, reduced the biases and standard deviations when compared with in-situ data from the World Ocean Database (WOD) [9]. For two regions in the California Current System and the Gulf Stream, considerable differences were found in regional SST gradients calculated from the Moderate Resolution Imaging Spectroradiometer (MODIS) and AVHRR data [10]. Similar results were also found in a study off the Peruvian-Chilean coast, a major upwelling region, where the order of magnitude differences in SST gradients were explained by differences in the resolution of the SST datasets [11]. Also off the Peruvian-Chilean coast, high-resolution numerical ocean models were used for validating remotely sensed SST gradients and revealed that SST gradients are related to changes in the seasonal upwelling cycle [12]. Other studies have shown the importance of using shipborne sensors and other instruments that can resolve the spatial variability to validate satellite-derived SST measurements [13]. Recently, a multi-stage trigonometric interpolation technique has been applied to determine the subpixel variability of satellite SST data, illustrating that this methodology could be used to examine the stripes in MODIS data, as well as possible features associated with cloud contamination [14]. In the Arctic Ocean, measurements from the Ball Experiment SST (BESST) thermal infrared radiometer were compared against MODIS data and revealed significant spatial variability within 1-km pixels that were associated with density fronts in the marginal ice zone [15]. Hence, methodologies must include understanding the subpixel scale variability, especially in areas of high spatial variability such as in upwelling and downwelling regions. Additionally, SST analyses are likely to perform differently depending on the environmental conditions [6], stressing the need for independent coastal validation.

Validation of SSS products has been a more recent research topic with the launch of the Aquarius mission, a collaboration between the National Aeronautics and Space Administration (NASA) and the Space Agency of Argentina (Comisión Nacional de Actividades Espaciales, CONAE), NASA's Soil Moisture Active Passive (SMAP) mission, and the European Space Agency's (ESA) Soil Moisture Ocean Salinity (SMOS) mission. With the launch of these missions and improvements in calibration, applications to coastal areas have provided opportunities to directly compare satellite-derived SSS with in-situ data. Traditionally, SSS has been validated on global scales while using ARGO [7,8]. Intercomparisons of the SMAP and SMOS data in both the Bay of Bengal and the Gulf of Mexico revealed standard deviation differences of less than 0.3 PSU [16,17]. A primary conclusion of the work was that satellite-derived SSS has the potential to observe freshwater plumes associated with river discharge. These studies [16,17] showed that vertical and horizontal gradients complicated the validation of SSS due to stratification. On a global scale, [18] found that biases were dependent on latitude but strongly increase near land masses. Results were based on comparisons with traditional pointwise measurements made by in-situ buoys. However, results are consistent in finding that biases and standard deviations increased at scales less than 100 km from land.

Overall, results from these studies point to the need for validation strategies in critical parts of the world's oceans, including the Arctic and coastal regions. Additionally, these strategies must go beyond traditional point measurements. Unmanned Surface Vehicles (USVs), such as Saildrone, provide new research opportunities. Saildrones provide a novel sampling technique that allows resolving mesoscale and submesoscale processes and thus to validate the capability of remote sensing data to capture the spatial variability observed in coastal regions. Saildrones provide in-situ sampling at high resolution (< 1 km). In this study, we validate satellite-derived SST and SSS measurements in a major coastal upwelling region off the California and Baja coast. This region was deliberately chosen as it is dominated by mesoscale to submesoscale variability associated with the California Current System [19, 20], providing a perfect test case for validating the performance of remote sensing tools to observe SST and SSS in regions with high oceanographic complexity. Although the Saildrone deployment measured other parameters such as ocean chlorophyll-a, the focus of this work was on SST and SSS, primarily because they both are available as gridded Level 4 (gapless) products. For SST, multi-sensor optimally interpolated Level 4 products are available through the Group for High Resolution Sea Surface Temperature (GHRSST), while SSS data are available as Level 3 products, but with few data gaps over an 8-day average. In contrast, chlorophyll-a has significant data gaps in the region due to persistent cloud cover, requiring more rigorous co-location strategies. That validation of the chlorophyll-a product is best left as a separate topic and focus.

2. Methods and Materials

2.1. Remote Sensing and Saildrone Data

2.1.1. Saildrone SSS and SST Data

Saildrone is a remotely-controlled wind and solar powered USV capable of long-distance deployments lasting up to 12 months and providing high quality, near real-time, multivariate surface-ocean and atmospheric observations while transiting at typical speeds of 3-5 knots. Data used in this work is from the California/Baja deployment in April-June of 2018. Although the saildrone measures several environmental variables, including air pressure, wind speed, oxygen, chlorophyll-a, humidity, air temperature, the focus of this work was to validate remotely sensed SSS and SST measurements. The SSS and SST measurements were both derived from the onboard conductivity, temperature, depth (CTD) sensors. Saildrones also carry an onboard Advanced Doppler Current Profiler (ADCP) which measures horizontal and vertical velocity.

The Saildrone Baja campaign consisted of a 60-day cruise from San Francisco Bay, down along the US/Mexico coast to Guadalupe Island and back again, over the period 11 April 2018 to 11 June 2018. Repeat surveys were taken around moored buoys operated by the National Data Buoy Center (NDBC). This Saildrone Baja dataset is comprised of one data file with the Saildrone platform telemetry and near-surface observational data (air temperature, sea surface skin and bulk temperatures, salinity, oxygen and chlorophyll-a concentrations, barometric pressure, wind speed and direction) for the entire cruise at 1-minute temporal resolution. A second file contains the ADCP current vector data that is depth-resolved to 100 m, at 2-m intervals, and binned temporally at 5-minute resolution. All data files are in netCDF format and CF/ACDD compliant consistent with the NOAA/NCEI specification. All the data and access to additional information about the instrument may be found at: https://podaac.jpl.nasa.gov/dataset/SAILDRONE_BAJA_SURFACE?ids=&values=&search=Saildrone. See also [21].

2.1.2. Remotely Sensed SSS Data

Three different remote sensing derived SSS datasets were used in the study: (1) the Jet Propulsion Laboratory version 4.0 Soil Moisture Active Passive (SMAP) (JPLSMAP) dataset; (2) the Remote Sensing Systems version 3.0 40 km (RSS40) dataset; and (3) the Remote Sensing Systems version 3.0 70 km (RSS70) dataset.

The JPLSMAP product has an inherent spatial resolution of 60 km. All the datasets were gridded at 25 km, with daily files produced as 8-day running means. The rationale for the 8-day averaging is that the SMAP satellite has an inherent repeat orbit of 8 days. Information on the JPLSMAP product may be found at: https://podaac.jpl.nasa.gov/dataset/SMAP_JPL_L3_SSS_CAP_MONTHLY_V4?ids=&values=&search=SMAP. More information on the retrieval algorithm and processing may be found in [22].

The RSS40 and RSS70 datasets have an inherent spatial resolution of 40 km and 70 km, respectively. The rationale for the two products was to allow for retrievals closer to land. The 40 km product allowed for retrievals closer to land, but with less smoothing than the lower resolution 70 km product. The 70 km product should be smoother. Both products are gridded at the same 25 km resolution. Specific information on the 40 km product may be found at https://podaac.jpl.nasa.gov/dataset/SMAP_RSS_L2_SSS_V3_40KM?ids=&values=&search=SMAP while the 70 km product may be accessed through https://podaac.jpl.nasa.gov/dataset/SMAP_RSS_L3_SSS_SMI_8DAY-RUNNINGMEAN_V3_70KM?ids=&values=&search=SMAP. Information on the processing of the RSS products may be found in [23]. User guides, as well as the Algorithm Theoretical Basis Document (ATBD) for these data sets, may be found under the docs directory (ftp://podaac-ftp.jpl.nasa.gov/allData/smap/docs/).

2.1.3. Remotely Sensed SST Data

Three different Level 4 SST products from the Group for High Resolution Sea Surface Temperature (GHRSST) were used in the study, the Multi-Scale Ultra-High Resolution (MUR) Sea Surface Temperature, the Operational Sea Surface Temperature and Sea Ice Analysis (OSTIA), and the Canadian Meteorological Center (CMC) Sea Surface Temperature data set.

The MUR SST data is a Level 4 product that uses wavelets in an optimal interpolation approach. Data from the Advanced Very High Resolution Radiometer (AVHRR), the Moderate Resolution Imaging Spectroradiometer (MODIS), the NASA Advanced Microwave Scanning Radiometer on EOS (AMSR-E), and the US Navy's Windsat are used in the processing of the Level 4 product. More details on the product may be found at: https://podaac.jpl.nasa.gov/dataset/MUR-JPL-L4-GLOB-v4.1?ids=&values=&search=%22MUR-JPL-L4-GLOB-v4.1%22. A detailed analysis of the algorithm and product validation may be found in [24].

The OSTIA SST is gridded at 5 km and is produced by the UK Meteorological Office. The different sensors used include AVHRR, the Spinning Enhanced Visible and Infrared Imager (SEVIRI), the Geostationary Operational Environmental Satellite (GOES) imager, the Infrared Atmospheric Sounding Interferometer (IASI), the Tropical Rainfall Measuring Mission Microwave Imager (TMI), and in-situ data from ships, drifting and moored buoys. More information on the OSTIA dataset may be found at: https://podaac.jpl.nasa.gov/dataset/OSTIA-UKMO-L4-GLOB-v2.0?ids=&values=&search=%22OSTIA-UKMO-L4-GLOB-v2.0%22. More information on the processing and algorithm may be found in [25].

The CMC SST data is provided by the Canadian Meteorological Office. Two versions have been produced at 20 km and 10 km. Currently, in the forward stream, only the 10 m gridded data is produced. That was the version used in this study. Sensors used in the Level 4 product include AVHRR from NOAA-18 and 19, the European Meteorological Operational-A (METOP-A) and Operational-B (METOP-B), and microwave data from the Advanced Microwave Scanning Radiometer 2 (AMSR2) onboard the GCOM-W satellite in conjunction with in-situ observations of SST from drifting buoys and ships from the ICOADS program. More information and data access may be found at: https://podaac.jpl.nasa.gov/dataset/CMC0.1deg-CMC-L4-GLOB-v3.0?ids=&values=&search=%22CMC0.1deg-CMC-L4-GLOB-v3.0%22. Additional information on processing and validation may be found in [26].

The REMSS product is produced at Remote Sensing Systems. The product merges both microwave and infrared data using optimal interpolation. Additionally, the product applies a diurnal model to account for day-night differences. Sensors used include: the microwave Global Precipitation Measurement (GPM) Microwave Imager (GMI), the Tropical Rainfall Measuring Mission (TRMM) Microwave Imager (TMI), the NASA Advanced Microwave Scanning Radiometer-EOS (AMSRE), the Advanced Microwave Scanning Radiometer 2 (AMSR2) onboard the GCOM-W1 satellite, WindSat on board of Coriolis satellite, infrared (IR) sensors such as the Moderate Resolution Imaging Spectroradiometer (MODIS) on the NASA Aqua and Terra platforms, and the Visible Infrared Imaging Radiometer Suite (VIIRS) on board the Suomi-NPP satellite. More information can be found at: https://podaac.jpl.nasa.gov/dataset/MW_OI-REMSS-L4-GLOB-v4.0?ids=&values=&search=REMSS or directly Remote Sensing Systems: http://dx.doi.org/10.5067/GHMWI-4FR03.

The NAVO K10 product is produced by the Naval Oceanographic Office (NAVOCEAN0). Microwave and infrared sensors are combined in an optimal interpolation. The following sensors are used: observations from the Advanced Very High Resolution Radiometer (AVHRR), the Advanced Microwave Scanning Radiometer for EOS (AMSR-E), and the Geostationary Operational Environmental Satellite (GOES) Imager. The analysis is tuned to represent SST at one meter. More information may be found at: https://podaac.jpl.nasa.gov/dataset/NAVO-L4HR1m-GLOB-K10_SST?ids=&values=&search=NAVO and http://dx.doi.org/10.5067/GHK10-41N01.

The DMI dataset is produced by the Danish Meteorological Institute. The sensors incorporated in the analysis include the Advanced Very High Resolution Radiometer (AVHRR), the Spinning Enhanced Visible and Infrared Imager (SEVIRI), the Advanced Microwave Scanning Radiometer 2

(AMSR2), the Visible Infrared Imager Radiometer Suite (VIIRS), and the Moderate Resolution Imaging Spectroradiometer (MODIS) on Aqua. For more information and data access go to: https://podaac.jpl.nasa.gov/dataset/DMI_OI-DMI-L4-GLOB-v1.0?ids=&values=&search=%22DMI_OI-DMI-L4-GLOB-v1.0%22 and http://dx.doi.org/10.5067/GHGDM-4FD02. More information on this product may be found found at [27].

2.2. Comparisons Between Satellite and Saildrone Data

The methodological approach considered in this work allowed us to examine the feasibility to use Saildrone data for evaluating the validation quality of satellite-derived SST and SSS data in coastal regions with high oceanographic complexity such as frontal activity. We compared values from three satellite-based SSS datasets derived from NASA's Soil Moisture Active Passive Mission (SMAP) and six SST datasets from the Group for High Resolution Sea Surface Temperature (GHRSST), against SSS and SST measurements from the remotely-controlled unmanned surface vehicle Saildrone. The primary goal here was not to validate each of these satellite-derived SST and SSS products individually, but to compare directly with Saildrone, thus validating the satellite-derived products in a coastal upwelling region. The process would highlight the use of Saildrone for coastal validation. Several types of calculations were derived in comparing the datasets. The three SMAP-derived SSS datasets used were the Jet Propulsion Laboratory 60 km product (JPLSMAP), the Remote Sensing System 40 km product (RSS40), and the Remote Sensing Systems 70 km product (RSS70). All these products are available through the Physical Oceanography Distributed Active Center (PO.DAAC) (http://podaac.jpl.nasa.gov) as described in the previous section.

The six GHRSST datasets selected for comparison were NASA's Multi-Scale Ultra-High Resolution SST (MUR), the UK Met Offices Operational Sea Surface Temperature and Sea Ice Analysis (OSTIA) SST data, the Canadian Meteorological Center's (CMC) SST data, The Naval Oceanographic (NAVOCEANO) K10 product, the Remote Sensing System (REMSS) product, and the Danish Meteorological Institutes (DMI) product. These are all gridded Level 4 products and were chosen to represent high resolution Level 4 gridded SST products and thus applicable for coastal regions. Details on these products are outlined in the 2.1.3.

Comparisons were done directly between the satellite-derived products and the Saildrone data. Biases, RMS differences, and overall signal-to-noise ratios were derived for each of the products. The bias was simply defined as:

$$BIAS = \sum_{1}^{N} (\mathrm{SAT} - \mathrm{SDRO})/\mathrm{N}, \quad (1)$$

where SAT is equal to one of the six parameters (JPLSMAP, RSS40, RSS70, MUR, OSTIA, and CMC), SDRO is the Saildrone SST or SSS, and N is the total number of matchups based on co-location criteria, between the SDRO and SAT along the Saildrone track. Co-locations were determined using a nearest-neighbor approach. For example, for MUR, the space-time window would be 1 km and 1 day. For the SSS products, the space-time window would be 25 km and 1 day. One day was used as the temporal co-location window, regardless of the smoothing used in the Level 3 (SSS) or Level 4 (SST) product.

SMAP SSS products were produced daily but consisted of 8-day running means. Thus co-location windows were defined by Level 3 gridding to be 25 km, and ± 1 day, regardless of the 8-day running mean.

The GHRSST SST datasets were also co-located based on a nearest-neighbor time-space window. The MUR SST data are gridded at 1 km, OSTIA at 5 km, CMC at 10 km, REMSS at 9 km, NAVO at 10km, and DMI at 5 km. Thus, the co-location space-time window was 1 km ± 1day for MUR, 5 km ± 1 day for OSTIA, 10 km ± 1 day for CMC, 9 km ± 1 day for REMSS, 10 km ± 1 day for NAVO, and 5 km ± 1 day for DMI. These co-location criteria were used for all the comparisons in this study. Co-locations were done for each Saildrone sample to not degrade the resolution of the Saildrone sampling. RMS differences were then calculated as follows:

$$RMSD = \sqrt{\sum_{1}^{N}(SAT - SDRO - BIAS)^2/N}, \quad (2)$$

where BIAS is the satellite-Saildrone bias defined in equation 1. To evaluate potential noise, when compared to Saildrone as the reference, the signal-to-noise ratio for each satellite parameter was derived as:

$$\frac{S}{N} = \frac{(\sqrt{\sum_{1}^{N}(SDRO - SDROMEAN)^2/N})}{RMSD} \quad (3)$$

where $\frac{S}{N}$ is the signal-to-noise ratio, and RMSD is the Root Mean Square Difference defined in equation 2.

Spectra and coherences were calculated for the different parameters to determine the relationship between the Saildrone and satellite data at the different spatial scales. The parameters included the following, the Saildrone SST and SSS data, RSS40 SSS, RSS70 SSS, JPLSMAP SSS, MUR SST, OSTIA SST, and CMC SST. Examining spectral slope is critical in coastal oceans where spatial scales can vary on the order of meters to 100s of kilometers.

A major question to be answered was how the observed differences between the satellite-derived products and Saildrone related to unresolved subpixel scale spatial variability. To further examine the differences between the satellite-derived products and Saildrone measurements, and their relationship to spatial scales, the wavelength spectra were examined for consistency with known spectral slopes defining mesoscale-submesoscale variability. Overall, the goal was to help relate these differences to possible issues of spatial resolution inherent to each dataset.

A first simple test was to compare the daily variability of the Saildrone data with the RMSD differences between the satellite-derived products and Saildrone. The question to be answered was whether the inherent daily variability of the Saildrone derived SST and SSS could explain these differences.

3. Results

3.1. Spatial and Temporal Representation

SST patterns from Saildrone, MUR, OSTIA, and CMC show a strong similarity with warmer waters off Southern California and the Baja Coasts (Fig. 1). All the SST data showed similar results. Thus only MUR, OSTIA, and CMC are shown as examples of the SST results. All products clearly show the cooler water along the coasts north of 32°N. These waters are associated with the coastal seasonal upwelling and are consistent with the known seasonal cycle [20,28]. All the products also show the strong gradient in SST south of 32°N. The CMC product shows slightly cooler SSTs along the westward track at 36°N. Statistical comparisons between these products are shown in section 3.2 Statistical Comparisons.

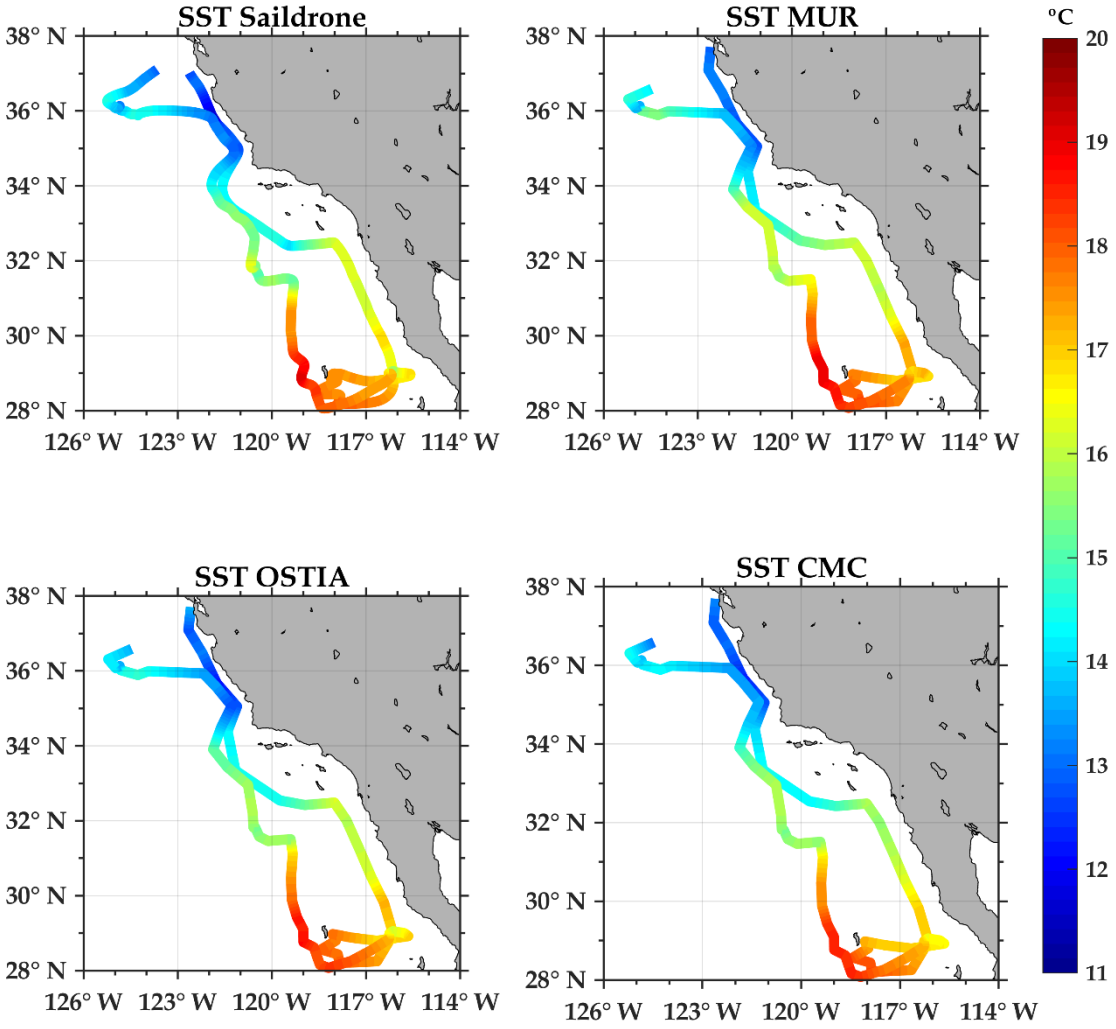

Figure 1. Sea surface temperature (SST) values from a Saildrone CTD, MUR, OSTIA, and CMC.

Compared to SST differences, larger differences are found between SSS measurements from the Saildrone, the JPLSMAP, RSS40, and the RSS70 product (Fig. 2). Clear gaps can be observed in the RSS70 product close to the coast, while the JPLSMAP product has complete coverage along the Saildrone track. Gaps in the RSS40 product also exist north of 34°N. Even before statistics are calculated between the products, one can visually determine a strong similarity between the Saildrone CTD SST and the satellite SST products, while the same imagery of the SSS indicates that pronounced biases exist between the products.

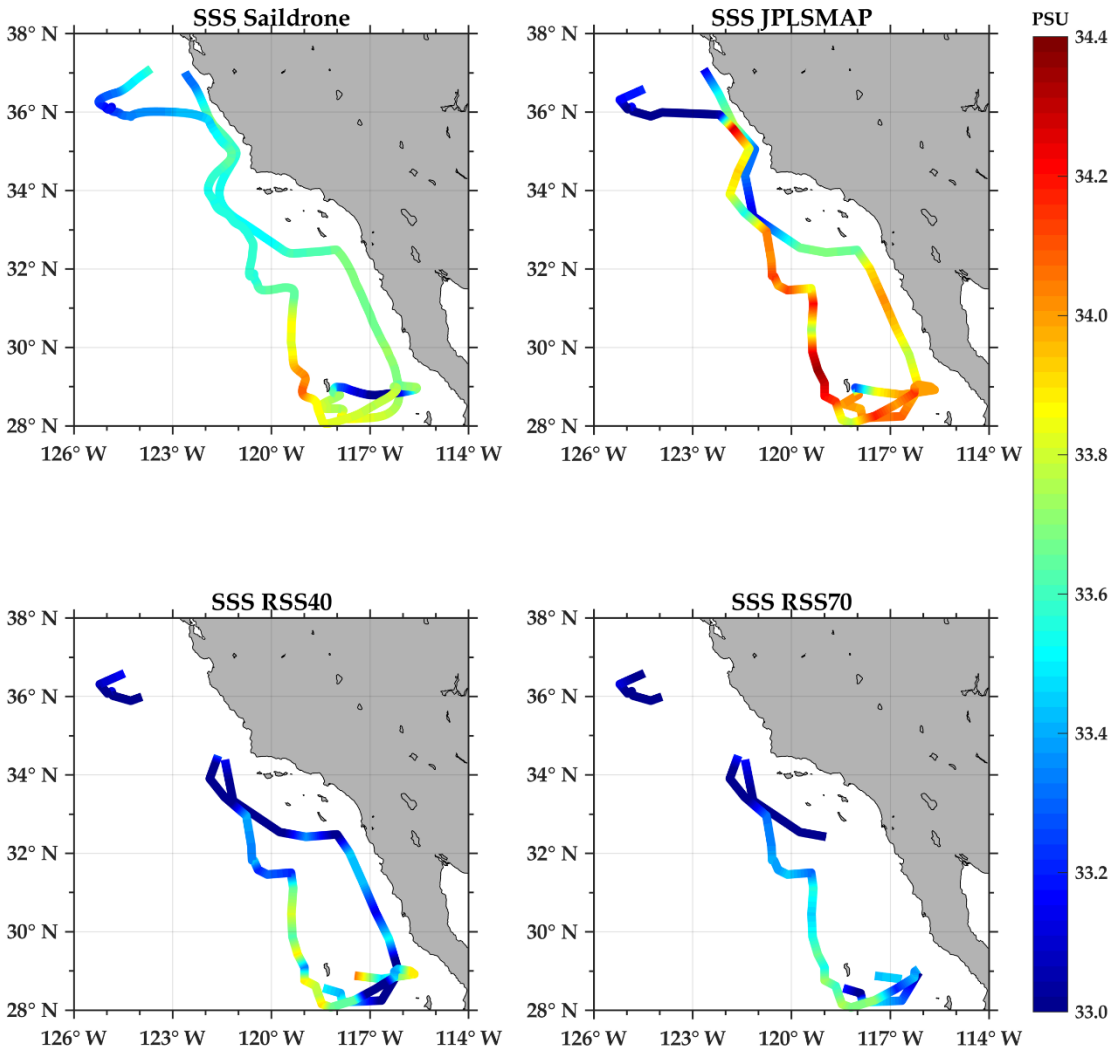

Figure 2. Sea surface salinity (SSS) from a Saildrone CTD, JPLSMAP, RSS40, and RSS70. The RSS40 and RSS70 products clearly show fresher biases near the coast.

Figure 3 below shows the time series of SST for Saildrone, MUR, OSTIA, and CMC along the Saildrone track. We deliberately only show results for MUR, OSTIA, and CMC, since results with DMI, K10, and REMSS were found to be similar. Thus MUR, OSTIA, and CMC were found to be representative of the statistics for the GHRSST Level 4 SST data.

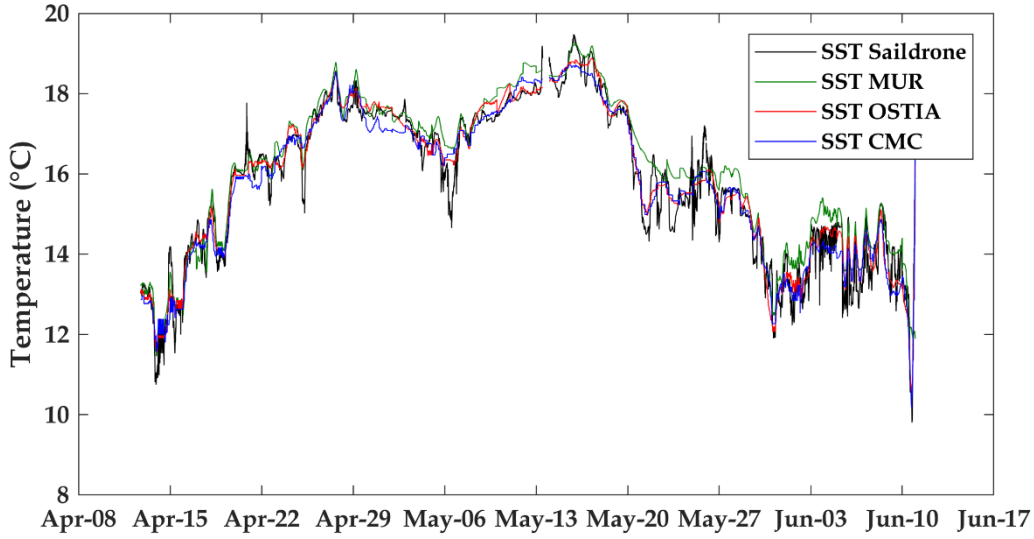

Figure 3. SST time series from Saildrone CTD, MUR, OSTIA, and CMC. MUR, OSTIA, and CMC are co-located to the Saildrone track.

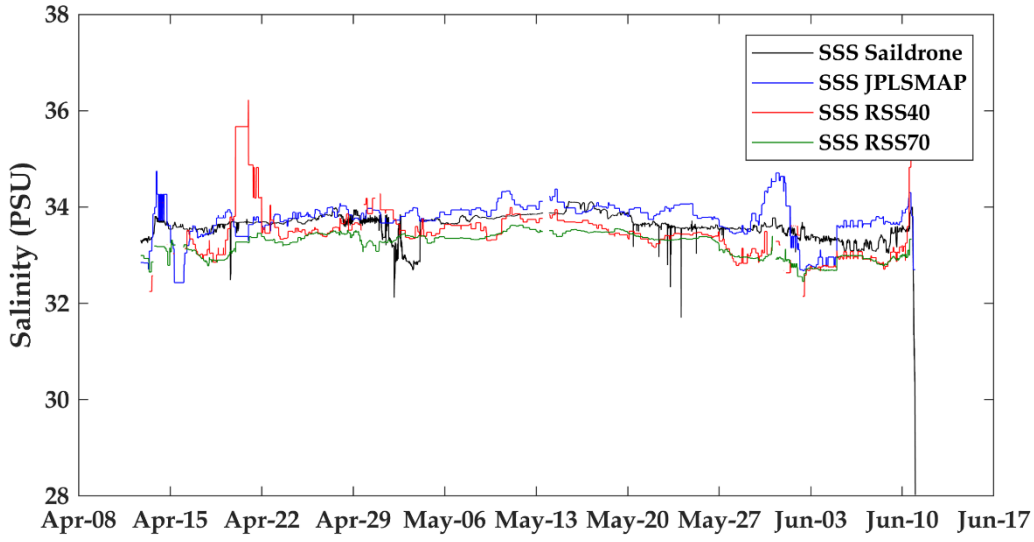

Figure 4. SSS time series from Saildrone CTD, JPLSMAP, RSS40, and RSS70.

Overall, the GHRSST L4 products follow the dominant features seen in the Saildrone data. There are clear indications though that there are periods of time when the differences are larger. In comparison to the SST results (Fig. 3), SSS values show larger overall differences with respect to the Saildrone data (Fig. 4). Differences of 1 PSU with respect to the Saildrone SSS are seen at different locations along with the deployment. Biases in the JPLSMAP product, in general, have an opposite sign (i.e., saltier) with respect to the RSS40, and RSS70 biases. Large biases are especially seen during May. The sign of the biases is consistent with the results found by [17] in the Gulf of Mexico. To further identify the possible relationship between the location of the biases and distance from the coast, difference plots were generated similar to Figures 1 and 2.

Figure 5 shows the differences between the different satellite SST products and Saildrone SST along the Saildrone track. The MUR data shows periods of warm biases greater than 1°C as the Saildrone track was furthest offshore. Both MUR and OSTIA show biases close to zero when the deployment was closest to shore. Possible explanations for these peaks in warm biases will be

discussed in the next section. Near-shore differences close to zero indicate that satellite-derived SST is doing well at resolving variability close to the coast.

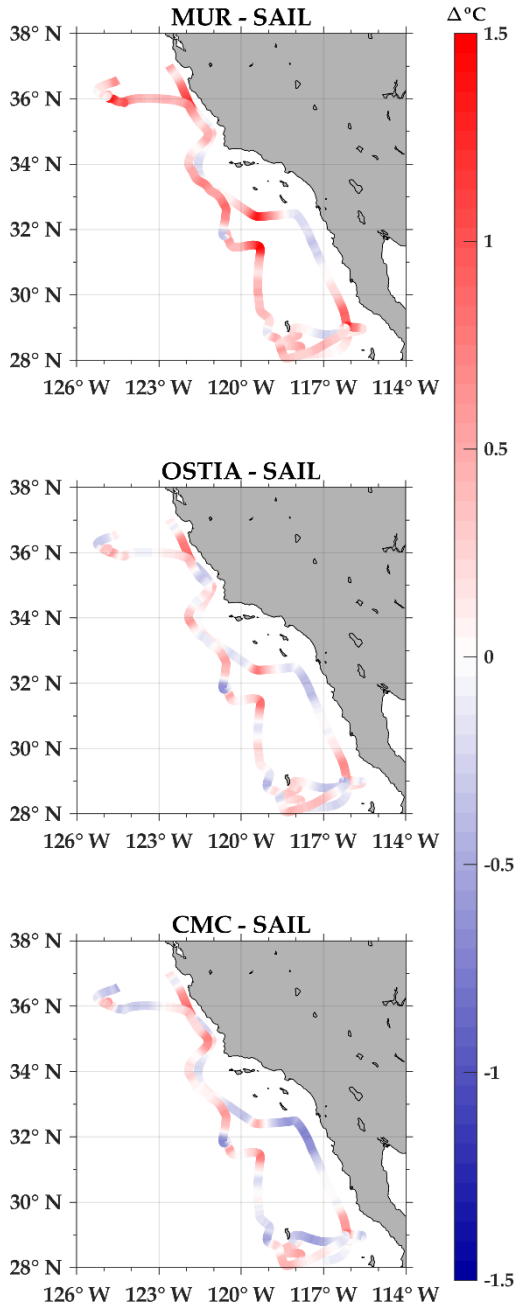

Figure 5. Difference plots for each of the remotely sensed SST products and the Saildrone-derived SST.

Figure 6 shows the difference plots for the SSS products. Saltier biases are found for the JPLSMAP product and fresh biases in the RSS40 and RSS70 products. The JPLSMAP product appears to show reduced biases closer to the coast, while saltier biases are seen further offshore. Overall, the RSS products show fresh biases along the entire Saildrone track.

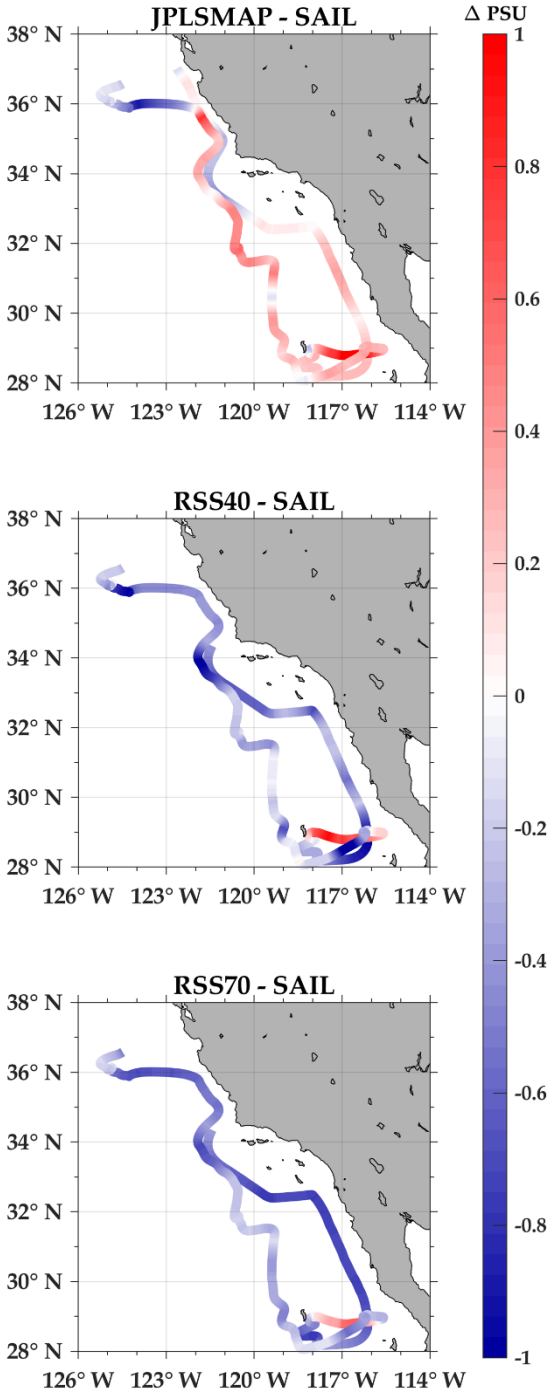

Figure 6. Difference plots for each of the remotely sensed SSS products and the Saildrone-derived SSS.

3.3. Statistical Comparisons

To summarize the results, statistics were calculated along the entire Saildrone track (Tables 1, 2, and 3). Results are shown for the entire deployment for correlation, bias, RMSD, and the signal-to-noise ratio. Overall, correlations for the three SST products with Saildrone SST are 0.97 to 0.98,

indicating a strong statistical relationship between values from the Saildrone SST and the satellite-derived products. These correlations suggest that the remote sensing SST products are resolving a significant amount of the variability associated with the Baja deployment. Biases for the OSTIA and CMC products were not significantly different from zero. OSTIA had the overall minimum RMSD of 0.39°C, while DMI showed the maximum RMSD of 0.5°C. MUR showed an overall warm bias of 0.3°C (Fig. 5). OSTIA showed the maximum signal-to-noise ratio of 6.2, while the minimum signal-to-noise ratio was found for K10. The high signal-to-noise ratios are consistent with the correlation values mentioned above (0.97).

Table 1. Correlation, Bias, RMSD, and signal-to-noise ratio for MUR, OSTIA, and CMC with respect to the Saildrone SST. REMSS, K10, and DMI products have been added for comparison.

Parameter	Bias (°C)	Standard Deviation (°C)	Correlation	Signal-to-Noise Ratio
CMC	-0.03	0.44	0.97	4.5
OSTIA	0.04	0.39	0.98	6.2
MUR	0.32	0.46	0.97	5.1
REMSS	0.11	0.43	0.97	4.4
K10	0.16	0.49	0.96	4.0
DMI	0.04	0.5	0.96	4.2

Table 2. Bias, RMSD, and Correlation between JPLSMAP, RSS40, RSS70, and the Saildrone derived SSS. All co-locations used.

Parameter	Bias (PSU)	RMSD (PSU)	Correlation
JPLSMAP	0.15	0.40	0.41
RSS40	-0.17	0.47	0.40
RSS70	-0.37	0.23	0.57

Table 3. Bias, RMSD, Correlation and Signal to Noise Ratio between JPLSMAP, RSS40, RSS70, and the Saildrone derived SSS. Only co-locations common to all three products were used.

Parameter	Bias (PSU)	RMSD (PSU)	Correlation	Signal-to-Noise
JPLSMAP	0.15	0.37	0.57	1.3
RSS40	-0.17	0.45	0.49	1.1
RSS70	-0.37	0.23	0.57	1.1

RMSD values between 0.3°C and 0.4°C in the MUR SST are consistent with the results from comparisons done by Chin et al. [24]. Considering the mesoscale to submesoscale variability associated with the California/Baja coast, the results compare well to other studies. The significance of these results will be discussed further in the next section. Overall, the high resolution of the SST data is contributing to resolving the high spatial variability along the California and Baja coasts.

Because the three satellite-derived salinity datasets (JPLSMAP, RSS40, and RSS70) had a different spatial coverage, two sets of statistics were calculated: one using only the points common to all three datasets (i.e., co-locations), and one using all the points. Co-locations (Methods and Materials) is based on the nearest neighbor for all the data sets. Spatial windows are based on the resolution of the Level 4 SST and Level 3 SSS data. For the SSS data that would be the nearest neighbor within the 25 km pixel. The largest impact on the statistics would be on the JPLSMAP product. Table 2 shows the results using all the co-locations for each product. Correlations with Saildrone values are

highest for RSS70 (0.57), while correlations with JPLSMAP and RSS40 are slightly weaker (0.4 and 0.47, respectively). The RSS70 had the smallest RMSD of 0.23 PSU while the JPLSMAP and RSS40 had RMSDs of 0.37 and 0.45 PSU, respectively. The JPLSMAP had a salty bias of 0.15 PSU while the RSS40 and RSS70 products had fresh biases of 0.17 and 0.37, respectively. Table 3 shows similar results, but only for the co-locations common to all three products. The major difference is in the improvement of the correlation for the JPLSMAP product. This is most likely due to the fewer points being used near the coast.

Statistics of the comparisons of the JPLSMAP, RSS40, and RSS70 SSS products with Saildrone SSS (correlations, biases, RMSD, and signal-to-noise ratios) indicate that the remote sensing derived SSS products are not reproducing the full spatial variability as well as for the SST products. Overall the JPLSMAP and RSS70 had the highest correlation of 0.57, with the RSS40 having a correlation of approximately 0.4. The JPLSMAP product had a salty bias of 0.15 PSU while the RSS40 and RSS70 products had a fresh bias of 0.2 and 0.3 PSU, respectively. The sign of the biases with respect to the different SSS products is consistent with results found by [17]. The RSS70 product had the smallest RMSD of 0.2 PSU, while the RSS40 product had an RMSD of 0.4 PSU. Signal-to-noise ratios were all close to 1 and significantly lower than found for the SST products. The overall statistics show major differences in the satellite-derived SSS products with respect to Saildrone.

4. Discussion

Differences between the Saildrone observations and satellite-derived SST and SSS products could be explained by the inherent capability of saildrones to resolve much higher spatial (sub-kilometer) and temporal (sub-daily) scales. The average daily variability of the Saildrone SST was 0.38 °C. Overall, this is approximately the mean RMSD between the satellite-derived products and Saildrone SST (Table 1). However, for SSS, the daily variability is 0.10 PSU, significantly lower than the RMSDs of 0.3 PSU between the satellite-derived SSS and Saildrone SSS (Table 2). Thus, for SSS, the differences cannot be simply explained by the daily variability of SSS as measured by Saildrone. This is also reflected in the higher signal-to-noise ratios for the SST products when compared to SSS. Thus, for SST, the differences can be explained by the unresolved spatiotemporal variability at the sub-daily and sub-kilometer scales. This could also include diurnal variability [29]. To examine the relationship between the satellite-derived parameters and the spatial scales, wavelength spectra and coherences were calculated for each of the SST and SSS products.

Figures 7 and 8 show the wavelength spectra for the Saildrone derived SST, MUR, OSTIA and CMC, as well as the SSS for Saildrone, JPLSMAP, RSS40, and RSS70.

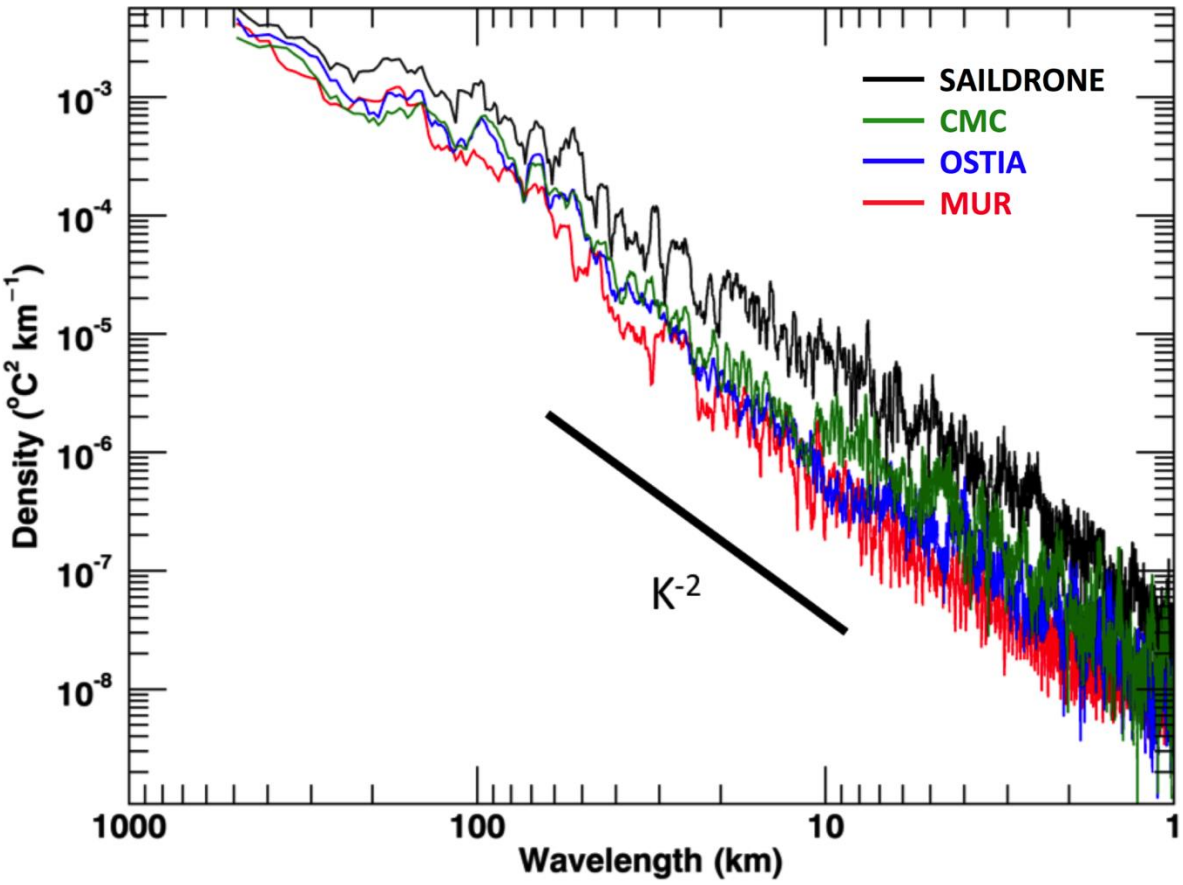

Figure 7. Power spectra for the three satellite-derived SST products and Saildrone SST. For the purpose of reference, the k^{-2} slope is overlaid.

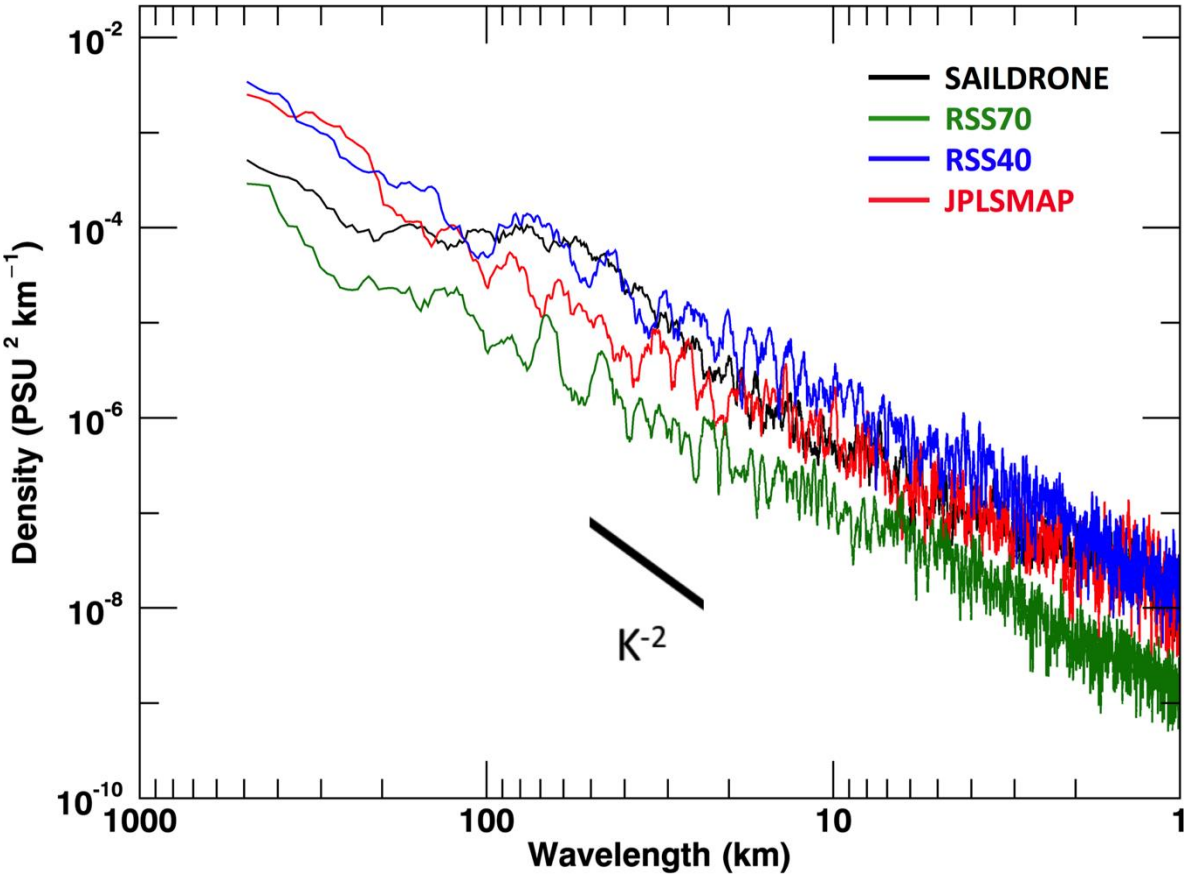

Figure 8. Power spectra for the three satellite-derived SSS products and Saildrone SSS. For the purpose of reference, the k^{-2} slope is overlaid.

Comparisons of the MUR, OSTIA, and CMC wavelength spectra with Saildrone indicate that satellite-derived products are resolving a significant part of the spatial variability in the region. Of course, this is for spatial scales greater than 20 km, the approximate Nyquist wavelength associated with the CMC product. Overall the Saildrone SST shows larger spatial variability, especially at scales smaller than 100 km associated with the mesoscale to submesoscale. The results of the SST spectra are consistent with the large signal-to-noise ratios in the direct comparison between values of the remote sensing SST products and Saildrone SST measurements.

Spectral slopes were calculated for the SST and SSS spectra (see Table 4). Overlaid on Figures 7 and 8 (as a reference) is the spectral slope of k^{-2}, which is used as a reference as it is commonly associated with power spectra resolving the mesoscale variability [15]. Table 4 summarizes the spectral slopes, based on the above spectra of the different SST and SSS products. All spectral slopes approximately followed the k^{-2} slope.

Table 4. Wavelength Spectral Slopes.

Parameter	(k^{-1})
SST Sail	-2.22
SST MUR	-2.11
SST OSTIA	-2.12
SST CMC	-2.12
SST REMSS	-1.92
SST DMI	-2.02
SST K10	-2.03
SSS Sail	-1.81
SSS JPLSMAP	-1.69
SSS RSS40	-1.96
SSS RSS70	-1.91

Slopes were derived from 500 km to 20 km, thus including the mesoscale and a portion of the submesoscale variability. The decision to examine the slope starting at 500 km was based on the approximate north-south distance of the Saildrone deployment. As a reference, Saildrone SST had a spectral slope of $k^{-2.2}$. OSTIA, CMC, and MUR all had spectral slopes of $k^{-2.1}$. Spectral slopes of k^{-2} to k^{-3} are consistent with the kinetic energy spectra for mesoscale to submesoscale variability [15,19]. [15] compared spectral slopes from MODIS Terra and Aqua, as well as an Unmanned Surface Vehicle (Ball Experimental Infrared Radiometer). They found spectral slopes of k^{-2} for wavelengths between 10 m and 100 km, thus encompassing primarily submesoscale variability. Spectral slopes for the REMSS, DMI, and K10 SST were more "white" than MUR, OSTIA, and CMC, but not statistically different. The relative consistency between the SST slopes indicates there were no major differences in the noise level inherent to the products. The SSS spectral slopes are also consistent with mesoscale to submesoscale variability. Saildrone, JPLSMAP, RSS40, and RSS70 SSS spectra had a slope of $k^{-1.8}$, $k^{-1.7}$, k^{-2}, and $k^{-1.9}$. Both the SST and SSS spectral slopes are consistent with results reported by [30], using a singularity method. Using data from ESA's Soil Moisture Ocean Salinity (SMOS) mission and OSTIA, they determined spectral slopes of $k^{-2.4}$ for wavelengths from 10000 km to 100 km. The overall magnitude of the wavelength spectra is consistent with previous results [15,19,30]. Based on the

consistency of the spectral slopes, both the SST and SSS are resolving scales associated with the mesoscale and submesoscale variability. The next analysis focused on the coherence to determine at what wavelengths the relationships between the satellite-derived products and Saildrone were significant.

Figures 9 and 10 show the coherence between the SST and SSS satellite-derived products and Saildrone. SST shows coherence close to 1 for spatial scales greater than 300 km, then a minimum before a local maximum at approximately 100 km (Fig. 9). MUR has the highest coherence value at 300 km, while OSTIA has the highest coherence value at 100 km. Error bars indicate that peaks at 300 km and 100 km are statistically significant. At spatial scales smaller than 30 km, coherences for all the products become statistically insignificant. Thus, at spatial scales associated with the submesoscale variability, the Saildrone SST is likely resolving oceanic structures and processes that are not captured in the satellite-derived products.

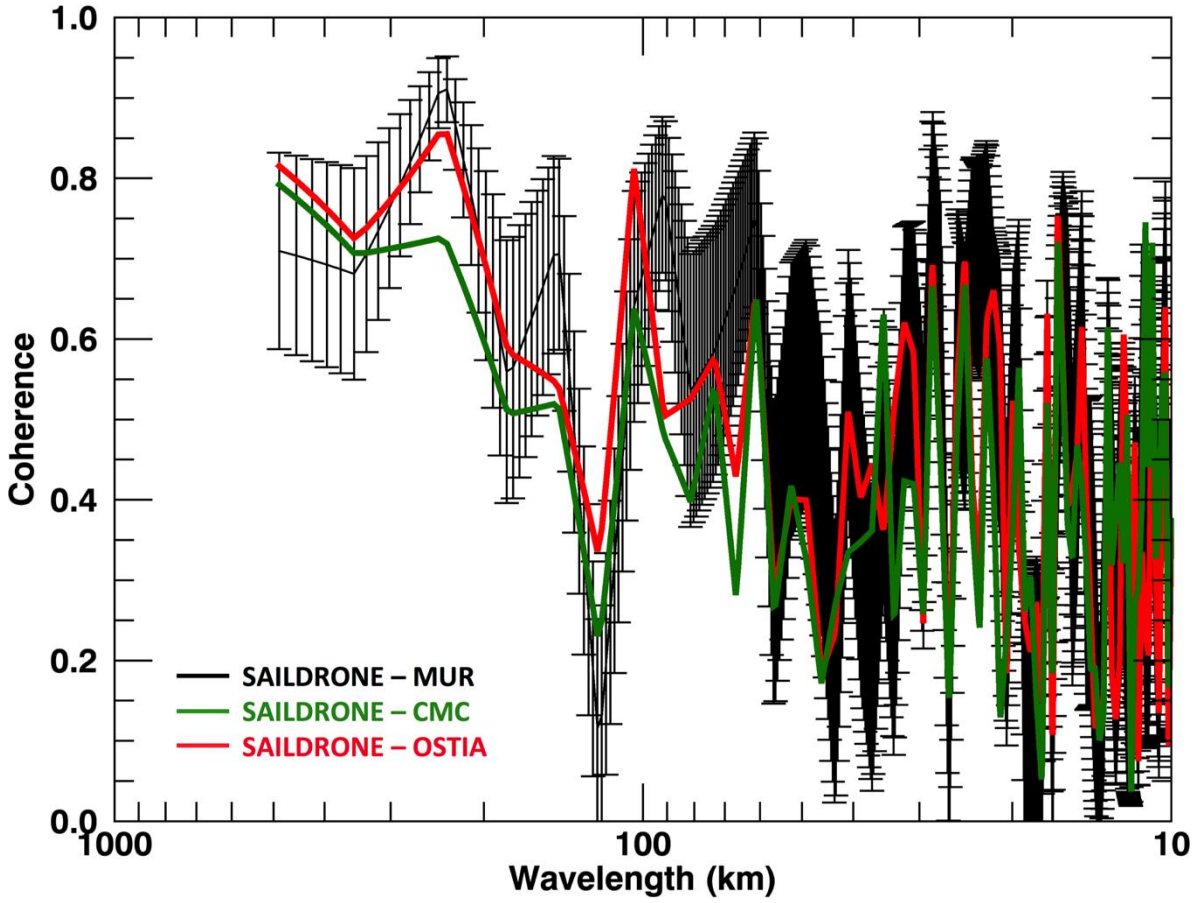

Figure 9. Coherences between the Saildrone SST and the SST from the MUR, OSTIA, CMC products.

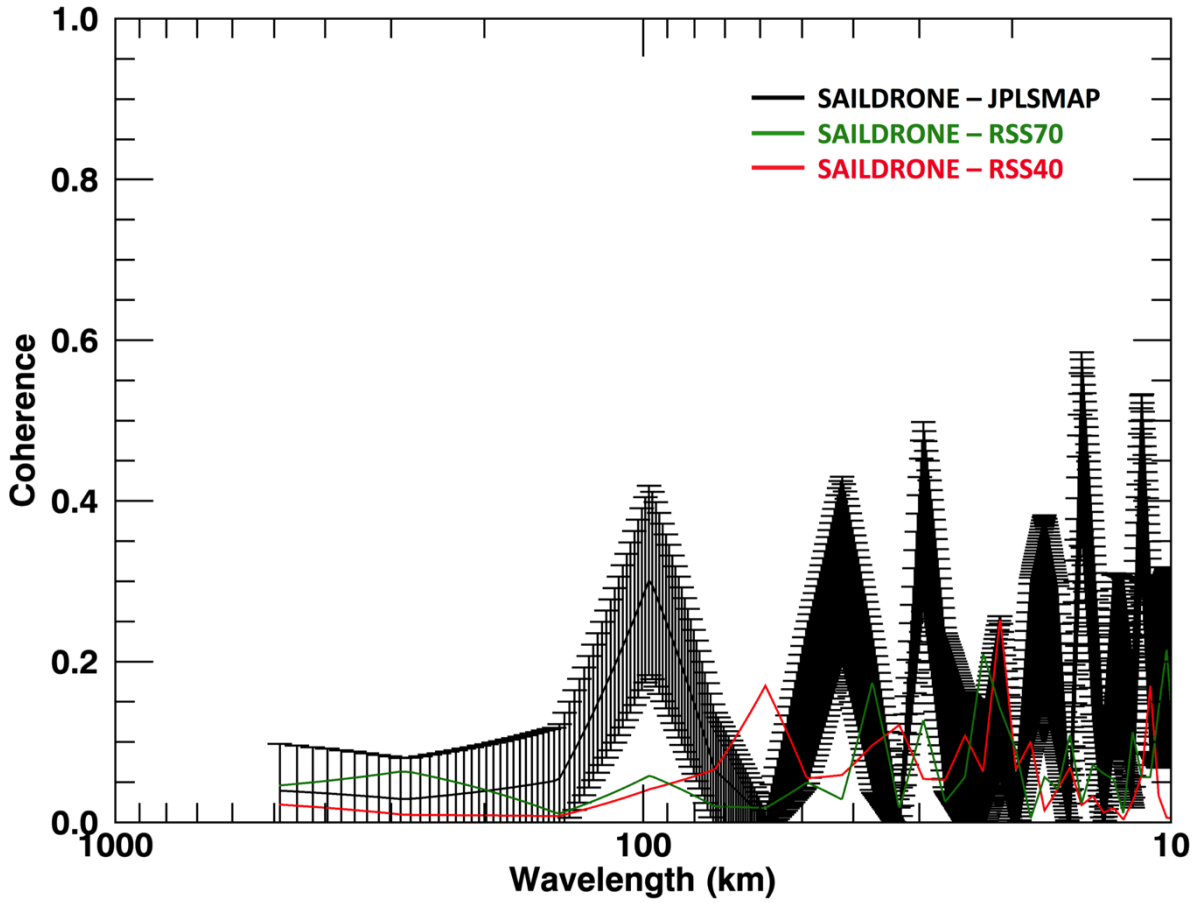

Figure 10. Coherences between the Saildrone SSS and SSS from JPLSMAP, RSS40, and RSS70 products.

SSS coherences show a statistically significant peak between the JPLSMAP and Saildrone SSS at 100 km (Fig. 10). As with SST, all the coherences become statistically insignificant at wavelengths less than 50 km. Again, this indicates that the satellite-derived products are not fully resolving the spatial scales associated with submesoscale variability. Overall the SST coherences are larger for scales of less than 100 km, but the error bars indicate that appropriate caution be taken in interpreting the significance of these findings.

The maxima in coherences at 100 km can best be understood by the coastal upwelling in the region [20]. A major difference in the two spectra is the lack of coherence in the SSS at spatial scales exceeding 100 km. This is most likely due to the data gaps that occur in the SSS products close to land. A detailed analysis is beyond the scope of this study. The SSS spectra show differences between the three products, especially at wavelengths of less than 100 km.

The peaks found at 100 km are very encouraging in showing that both satellite-derived SST and SSS are coherent at scales associated with mesoscale turbulence in the California Current System [19,20]. The upwelling system along the Californian coast, in general, is within 25 km of the coast, but the influence can be much larger. Thus, the maxima in coherence seen at 100 km would be consistent with both the influence of upwelling along the California Coast as well as the inherent resolutions and Nyquist wavelengths of the datasets. For example, the Nyquist wavelength would be 120 km for the JPLSMAP product, 80 km for RSS40, and 140 km for RSS70. The SST spectra show statistically significant coherences at wavelengths smaller than 100 km, consistent with the higher resolution of the SST data and the ability in resolving smaller spatial scales. However, the error bars indicate that neither the SST or SSS satellite-derived products are fully resolving the variability associated with the submesoscale.

5. Conclusions

Results from in this study present the first known validation of satellite-derived SSS and SST measurements off the California and Baja coasts, using a USV. Overall correlations of Saildrone SST with SST values from MUR, OSTIA, CMC, REMSS, K10, and DMO products exceed 0.97. OSTIA and CMC show biases that are close to zero, with MUR showing positive biases of 0.3°C, RMSD differences are consistent with other validation studies on regional to global scales. The consistency of RMSD off the California/Baja coasts with global comparisons is promising for applications of high-resolution SST retrievals in coastal regimes. Coherences between MUR, OSTIA, CMC and the Saildrone SST are close to one at the longer wavelengths with a minimum at approximately 200 km before increasing again at 100 km.

Results for SSS and the comparisons of Saildrone SSS with the JPLSMAP, RSS40, and RSS70 satellite-derived products are encouraging, but not as statistically significant as for SST. Most likely this is due to two issues: (1) the lower spatial resolution of the SSS satellite-derived data; (2) land contamination. Land contamination results as part of the satellite footprint are over land. For both SMAP and SMOS this occurs at distances less than 100 km from land. Overall the highest correlation (approximately 0.6) was found between Saildrone SSS and the JPLSMAP product, while the lowest correlation (0.4) was found for the RSS40 product. Results are consistent with the RSS40 product having the least spatial smoothing, thus more noise, but the highest spatial resolution. This is consistent with the lower S/N ratio. The RSS70 product shows the lowest RMSD around 0.3 PSU, while the RSS40 product shows the highest RMSD at approximately 0.4 PSU. Additionally, when RMSD values of satellite minus Saildrone are compared with the daily variability of SSS and SST observations from Saildrone, the RMSD for SST can be explained by the unresolved daily variability. However, for SSS, RMSD values are significantly larger, indicating the increased noise and/or possible land contamination of the satellite-derived SSS products. Results are encouraging though that the RMSD of 0.3 PSU is only slightly higher than RMSD values of global comparisons of 0.2 PSU [3]. Coherences show a peak at 100 km (same as SST), but become statistically insignificant at wavelengths <100 km.

With this work, we intend to illustrate the potential of using USVs for validating remotely sensed ocean data in coastal regions. Future work will focus on applications of remote sensing data in challenging regimes while incorporating Saildrone to validate the satellite products and the relationship to mesoscale submesoscale features.

Acknowledgments: The research described in this paper was carried out at the Jet Propulsion Laboratory, California Institute of Technology, under a contract with the National Aeronautics and Space Administration (NASA). This research was supported by the NASA Science Utilization of the Soil Moisture Active-Passive Mission Salinity Continuity program as well as the National Ocean Partnership Program. Data for this paper are available at the Physical Oceanography Distributed Active Center (PO.DAAC (http://podaac.jpl.nasa.gov).

Author Contributions: All the authors played a critical part in the preparation of the manuscript. Each author brought their expertise, including scientific expertise in the California Coast and Baja Coasts.

Funding: This research was supported by NASA Salinity Continuity Program as well as the National Ocean Partnership Program (NOPP) Multi-Sensor Improved Sea Surface Temperature (MISST) Program. JGV and LEM were supported by CICESE and CONACYT, grant # 257125, México.

Conflicts of Interest: The authors declare no conflict of interest.

6. References

1. Zhang, Z.; Wang, W.; Qui, B. Oceanic mass transport by mesoscale eddies. *Science* **2014**, *345*, 322–324.
2. Falkowski, P.G.; Ziemann, D.; Kolber, Z.; Bienfang, P.K. Role of eddy pumping in enhancing primary production in the ocean. *Nature* **1991**, *352*, 55–58.
3. Doddridge, E.W.; Marshall, D.P. Implications of eddy cancellation for nutrient distribution within subtropical gyres. *J. Geophys. Res. Oceans* **2018**, *123*, 6720–6735.

4. Hausmann, U.; Czaja, A. The observed signature of mesoscale eddies in sea surface temperature and the associated heat transport. *Deep-Sea Res. 1 Oceanogr. Res. Pap.* **2012**, *70*, 60–72.
5. Melnichenko, O.; Amores, A.; Maximenko, N.; Hacker, P.; Potemra, J. Signature of mesoscale eddies in satellite sea surface salinity data. *J. Geophys. Res. Oceans* **2017**, *122*, 1416–1424.
6. Castro, S.L.; Wick, G.A.; Steele, M. Validation of satellite sea surface temperature analyses in the Beaufort Sea using UpTempO buoys. *Remote Sens. Environ.* **2016**, *187*, 458–475.
7. Tang, W.; Fore, A.; Yueh, S.; Lee, T.; Hayashi, A.; Sanchez-Franks, A.; Martinez, J.; King, B.; Baranowski, D. Validating SMAP SSS with in-situ measurements. *Remote Sens. Environ*. **2017**, *200*, 326–340.
8. Lee, T. Consistency of Aquarius sea surface salinity with Argo products on various spatial and temporal scales. *Geophy. Res. Lett.*, **2016**, *43*, 3857–3964.
9. Vazquez-Cuervo, J.; Armstrong E.M.; Casey, K.S.; Evans, R.; Kilpatrick, K. Comparison between the Pathfinder Versions 5.0 and 4.1 Sea Surface Temperature Datasets: A Case Study for High Resolution. *J. Clim.* **2010**, *23*, 1047–1059.
10. Armstrong, E.M.; Wagner, G.; Vazquez-Cuervo, J. Comparisons of regional satellite sea surface temperature gradients derived from MODIS and AVHRR sensors. *Int. J. Remote Sens.* **2012**, *33*, 6639–6651.
11. Vazquez-Cuervo, J.; Dewitte, B.; Chin, T.M.; Armstrong, E.M. An analysis of SST gradients off the Peruvian Coast: The impact of going to higher resolution. *Remote Sens. Environ.* **2013**, *131*, 76–84.
12. Vazquez-Cuervo, J; Torres, H.S.; Menemenlis, D.; Chin, T.; Armstrong, E.M. Relationship between SST gradients and upwelling off Peru and Chile: model/satellite data analysis. *Int. J. Remote Sens.* **2017**, *38*, 6500–6622.
13. Castro, S.L.; Wick, G.A.; Minnett, P.J.; Jessup, A.T.; Emery, W.J. The impact of measurement uncertainty and spatial variability on the accuracy of skin and subsurface regression-based sea surface temperature algorithms. *Remote Sens. Environ.* **2010**, *114*, 2666–2678.
14. Castro, S.L.; Monzon, L.A.; Wick, G.A.; Lewis, R.D.; Beylkin, G. Subpixel variability and quality assessment of satellite sea surface temperature data using a novel High Resolution Multistage Spectral Interpolation (HRMSI) technique. *Remote Sens. Envron.* **2018**, *217*, 292–208.
15. Castro, S.L; Emery, W.J.; Wick, G.A.; Tandy, W. Submesoscale Sea Surface Temperature Variability from UAV and Satellite Measurements. *Remote Sens.* **2017**, *9*, 1089.
16. Boutin, J.; Chao, Y.; Asher,W.E.; Delcroix, T.; Drucker, R.; Drushka, K.; Kolodziejczyk, N.; Lee, T.; Reul, N.; Reverdin, G.; Schanze, J.; Soloviev, A.; Yu, L.; Anderson, J.; Brucker, L.; Dinnat, E.; Santos-Garcia, A.; Jones, W.L.; Maes, C.; Meissner, T.; Tang, W.; Vinogradova, N.; Ward, B. Satellite and in situ salinity: Understanding near-surface stratification and sub footprint variability. *Bull. Am. Meteorol. Soc.* **2016**, *97*, 1391–1407.

17. Vazquez-Cuervo, J; Fournier, S.; Dzwonkowski, B.; Raeger, J. Intercomparison of In-Situ and Remote Sensing Salinity Products in the Gulf of Mexico, a River-Influenced System. *Remote Sens.* **2018**, *10*, 1590.
18. Boutin, J.; Vergely, J.L.; Marchand, S.; D'Amico, F.; Hasson, A.; Kolodziejczyk, N.; Reul, N.; Reverdin, G.; Vialard, J. New SMOS Sea Surface Salinity with reduced systematic errors and improved variability. *Remote Sens. Environ.* **2018**, *214*, 115–134.
19. Capet, X.; McWilliams, J. C.; Molemaker, M. J.; Shchepetkin, A. F. Mesoscale to submesoscale transition in the California Current System. Part I: Flow structure, eddy flux, and observational tests. *J. Phys. Oeanogr.* **2008**, *38*, 29–43.
20. Garcia-Reyes, M.; Largier, J.L. Seasonality of coastal upwelling off central and northern California: New insights, including temporal and spatial variability. *J. Geophys. Res.* **2012**, *117*, C03028.
21. Saildrone. 2018. Saildrone Baja field campaign surface and ADCP measurements. Ver. 1.0. PO.DAAC, CA, USA. Dataset accessed [2019-12-19] at http://dx.doi.org/10.5067/SDRON-SURF0.
22. Fore, A.G; Yueh, S.H.; Tang, W.; Stiles, B.W.; Hayashi, A.K. Combined Active/Passive Retrievals of Ocean Vector Wind and Sea Surface Salinity with SMAP. *IEEE Transactions on Geoscience and Remote Sensing* **2016**, *54*, 7396–7404.
23. Meissner, T. and F. J. Wentz, **2016**: Remote Sensing Systems SMAP Ocean Surface Salinities, Version 2.0 validated release. Remote Sensing Systems, Santa Rosa, CA, USA.
24. Chin, T.M.; Vazquez-Cuervo, J.; Armstrong, E.M. A multi-scale high-resolution analysis of global sea surface temperature. *Remote Sens. Environ.* **2017**, 200, 154–169.
25. Donlon, C.J.; Martin, M.; Stark, J.; Roberts-Jones, J.; Fiedler, E.; Wimmer, W. The Operational Sea Surface Temperature and Sea Ice Analysis (OSTIA) system. *Remote Sen. Env.* **2012**, *116*, 140–158.
26. Brasnett, B. The impact of satellite retrievals in a global sea-surface-temperature analysis. *Q.J.R. Meteorol. Soc.* **2008**, *134*, 1745–1760.
27. Høyer, J.L.; Le Borgne, P.; Eastwood, S. A bias correction method for Arctic satellite sea surface temperature observations. *Remote Sens. Environ.* **2013**, *146*, 201–213.
28. Huyer, A. Coastal upwelling in the California Current System. *Prog. Oceanogr.* **1983**, *12*, 259–284.
29. Gentemann, C.L.; Donlon, C.J.; Stuart-Menteth, A.; Wentz, F. Diurnal signals in sea surface temperature measurements. *Geophys. Res. Lett.* **2003**, *30*, 1140.
30. Hoareau, N.; Turiel, A.; Portabella, M.; Ballabrera-Poy, J.; Vogelzang, J. Singularity Power Spectra: a method to assess geophysical consistency of gridded products-application to sea-surface salinity remote sensing maps. *IEEE Transactions on Geoscience and Remote Sensing* **2018**, *56*, 5525–5536.